ELSEVIER

Journal of Nuclear Materials 288 (2001) 57–65

journal of nuclear materials

www.elsevier.nl/locate/jnucmat

Thermal conductivities of irradiated UO_2 and $(U,Gd)O_2$

K. Minato [a,*], T. Shiratori [a], H. Serizawa [a], K. Hayashi [a], K. Une [b,1], K. Nogita [b,2], M. Hirai [b,1], M. Amaya [b,1]

[a] *Department of Chemistry and Fuel Research, Japan Atomic Energy Research Institute, Tokai-mura, Naka-gun, Ibaraki-ken 319-1195, Japan*

[b] *Nippon Nuclear Fuel Development Co., Ltd. 2163, Narita-cho, Oarai-machi, Higashi-ibaraki-gun, Ibaraki-ken 311-1313, Japan*

Received 10 April 2000; accepted 15 October 2000

Abstract

The evaluation of thermal conductivity of irradiated fuel is very important since it directly affects the fuel operating temperature. The disk-shaped UO_2 and UO_2–10 wt%Gd_2O_3 samples were prepared and irradiated to about 4%FIMA to measure the thermal diffusivities by the laser flash method. The burnup was almost uniform within each sample. The irradiation temperature was almost constant and uniform within each sample except the temperature escalation that occurred during the irradiation. The thermal conductivity, determined from the thermal diffusivity, density and specific heat capacity, decreased by irradiation, while it partly recovered after the thermal diffusivity measurement at temperatures up to about 1800 K. The thermal conductivity reduction attributable to the irradiation-induced point defects was small in the samples which experienced higher temperature than 1273 K during the temperature escalation. The present results were compared with the reported models.

PACS: 66.70.+f

1. Introduction

Thermal conductivity is one of the most important properties of nuclear reactor fuel pellets, which directly influences the fuel operating temperature, since the fuel performance and behavior such as the fission gas release and swelling are affected by the fuel operating temperature. Although the thermal conductivity measurements of UO_2 pellets were made particularly in the 1960s whose data were critically reviewed and analyzed [1–4], parametric dependence of the thermal conductivity of UO_2 on irradiation-induced character changes was not well clarified yet.

In recent years, increase in the target burnup of the fuel of light-water reactors has made it more important to evaluate the thermal conductivity of irradiated fuels since the thermal conductivity of fuel decreases by irradiation. To develop a model of the thermal conductivity of irradiated fuels, measurements of the thermal diffusivities of unirradiated fuels [5–7], of simulated burnup fuels [8–12] and of irradiated fuels [13–16] were made by a laser flash method. In the analytical models proposed, parameters such as the burnup, porosity, deviation from stoichiometry, radiation damage were taken into account [13,17–19]. To verify the models, the data of the thermal conductivity of well-characterized irradiated fuels are needed. However, only a few published data are available on the thermal conductivity of irradiated UO_2 measured by the laser flash method [13–16], while there are some data obtained by in-reactor measurements [20–22]. No published data are available

* Corresponding author. Tel.: +81-29 282 5402; fax: +81-29 282 6442.

E-mail address: minato@popsvr.tokai.jaeri.go.jp (K. Minato).

[1] Present address: Japan Nuclear Fuel Co., Ltd., 2163, Narita-cho, Oarai-machi, Higashi-ibaraki-gun, Ibaraki-ken 311-1313, Japan.

[2] Present address: Department of Mining, Minerals and Materials Engineering, University of Queensland, Brisbane QLD 4072, Australia.

0022-3115/01/$ - see front matter
PII: S0022-3115(00)00578-X

on the thermal conductivity of irradiated $(U,Gd)O_2$ solid solution.

In the present study, disk-shaped UO_2 and $(U,Gd)O_2$ samples were prepared and irradiated to measure the thermal diffusivities by the laser flash method. As the disk-shaped samples were used instead of cylindrical pellets, no sample preparation after the irradiation was needed for the thermal diffusivity measurement. Furthermore, distributions of the irradiation temperature and burnup within the samples could be kept flat by using a specially designed irradiation capsule. The thermal conductivities were determined from the measured thermal diffusivities and densities and the specific heat capacities in the literature.

2. Experimental

2.1. Samples

The samples used for the thermal diffusivity measurement were three irradiated UO_2 disks and one irradiated $(U,Gd)O_2$ disk, together with one unirradiated UO_2 disk and one unirradiated $(U,Gd)O_2$ disk for comparison. The disk samples were fabricated at the Nippon Nuclear Fuel Development (NFD) and irradiated in the Japan Research Reactor-3M (JRR-3M) at the Japan Atomic Energy Research Institute (JAERI). Characteristics of the disks are shown in Table 1. The unirradiated disks of samples H-std and F-std were fabricated in the same batches as samples H-4 and F-3, respectively. The dimensions of each disk were 3 mm in diameter and 1 mm in thickness. Fig. 1 shows a stereomicrograph of the irradiated disk (D-4) as a typical example. Gadolinium used was 98.6% enriched ^{160}Gd, which contained very small fractions of ^{155}Gd and ^{157}Gd having large neutron capture cross-sections, to avoid burnup depression. This character is reasonable for a study of the irradiation effects on the thermal conductivity of $(U,Gd)O_2$.

The disk samples for the thermal diffusivity measurement, together with square-shaped samples (2.4 mm × 2.4 mm × 1 mm) for the other experimental objectives, were irradiated in a closed capsule. The samples were encased individually in molybdenum holders, as shown in Fig. 2, which were enclosed in Zr–1%Nb tubes with helium gas to fabricate fuel pins. Eleven fuel pins, containing 16 samples each, were inserted into molybdenum blocks. The fuel pins, together with the molybdenum blocks, were held within two containment tubes. Helium gas was sealed in the primary tube. The operating temperatures were regulated by changing the composition and pressure of helium/neon gas contained between the primary and the secondary containment tubes. The irradiation temperatures

Table 1
Characteristics of samples

Name	As-fabricated samples						Irradiated samples			
	Composition	O/M ratio[a]	^{235}U enrichment (wt%)	Grain size (μm)	Sample density (Mg/m^3)	Theoretical density (Mg/m^3)	Burnup (%FIMA)	Sample density (Mg/m^3)	Theoretical density[b] (Mg/m^3)	Lattice parameter (pm)
H-std	UO_2	2.001	3.9	12	10.65	10.96	–	–	–	547.02[c]
H-4	UO_2	2.001	3.9	12	10.65	10.96	1.84	10.47	10.90	547.76
D-4	UO_2	2.000	8.0	10	10.58	10.96	4.07	10.11	10.84	547.07
E-17	UO_2	2.001	8.0	61	10.57	10.96	4.07	10.11[d]	10.84	547.02
F-std	UO_2–10 wt%Gd_2O_3	1.983	8.0	51	10.21	10.62	–	–	–	544.56[c]
F-3	UO_2–10 wt%Gd_2O_3	1.983	8.0	51	10.21	10.62	4.12	9.98	10.52	544.89

[a] Determined by spectrophotometric method.
[b] Estimated after Ishimoto et al. [11].
[c] Value for unirradiated sample.
[d] Estimated from sample D-4.

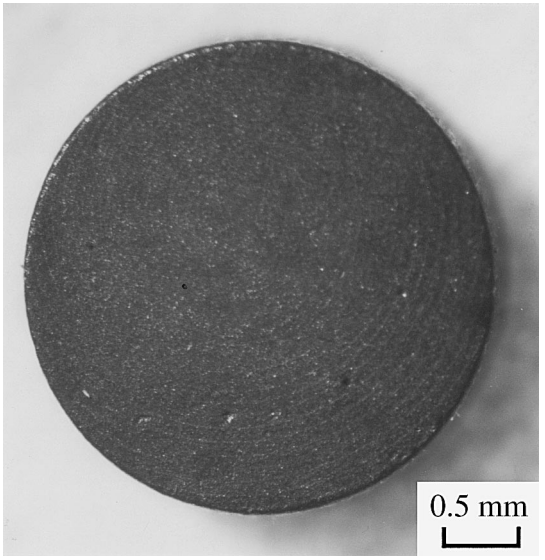

Fig. 1. Stereomicrograph of irradiated UO_2 disk sample of D-4 for thermal diffusivity measurement.

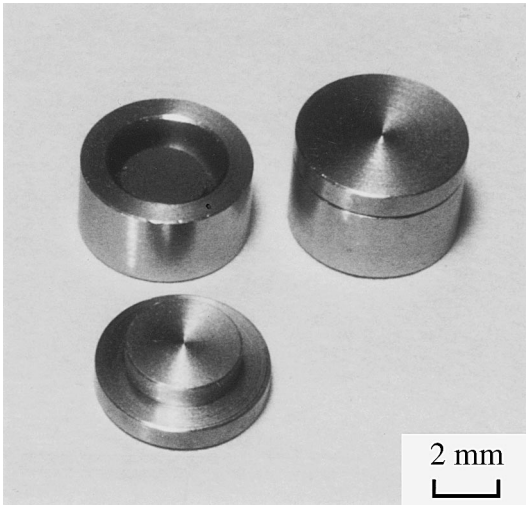

Fig. 2. Stereomicrograph of the sample holders with a disk sample.

were monitored at the molybdenum blocks with thermocouples of the type K.

The irradiation duration was 232.1 effective full power days (EFPD). The irradiation temperatures of the samples were regulated well to 207.1 EFPD, while a temperature escalation occurred after that on account of an inadequate operation of the temperature regulation system. After the temperature escalation, the temperature was maintained below 573 K from 214.1 to 232.1 EFPD, as shown in Table 2.

2.2. Procedure

2.2.1. Characterization of irradiated samples

For characterization of the irradiated samples, square-shaped samples of the same kind and of the same irradiation conditions as the disks were used; the disks listed in Table 1 were used only for the thermal diffusivity measurement. The square-shaped sample that was equivalent to the disk H-4, for example, was named $H\text{-}4_{eq}$.

The burnup of each sample was determined by means of mass spectrometric measurement of ^{148}Nd and uranium and plutonium isotopes after chemical treatment of the samples. The immersion density of each sample was measured using methylene iodide. The burnup and density determined are shown in Table 1. The polished surfaces of the samples were observed with an optical microscope and the profiles of fission product distributions on the polished surfaces were measured with an electron probe microanalyzer. Two different sections of polished surfaces were prepared for the examinations; a horizontal cross-section (2.4 mm × 2.4 mm) and a vertical cross-section (1 mm × 2.4 mm). Lattice parameters of the samples were determined with X-ray diffractometry using polished samples.

2.2.2. Determination of thermal conductivity

The thermal diffusivities of UO_2 and UO_2–10 wt%Gd_2O_3 were measured on the disk samples by the laser flash method. The apparatus used for the thermal diffusivity measurement has been described elsewhere [23]. For the measurement, the disk sample was set in the

Table 2
Irradiation conditions of samples

Name	Duration (EFPD)	Temperature (K)		
		Steady state[a]	Escalation[b]	Post-escalation[c]
H-4	232.1	863–723	<1273	<573
D-4	232.1	923–823	>1273	<573
E-17	232.1	923–823	>1273	<573
F-3	232.1	923–823	>1273	<573

[a] Temperature from 0 to 207.1 EFPD.
[b] Maximum temperature during temperature escalation from 207.1 to 214.1 EFPD.
[c] Temperature from 214.1 to 232.1 EFPD.

apparatus and heated to the desired temperatures with a tungsten heater, where the sample temperature was measured with a thermocouple of the type W–5%Re/W–26%Re placed near the sample. The measurements were performed from room temperature to about 1800 K at intervals of about 100 K in vacuum below 1×10^{-3} Pa. At each temperature, the measurements were repeated three times.

The thermal diffusivity was determined from the temperature rise at the rear surface measured with an In–Sb infrared detector after the front surface of the sample was heated by the pulse of a ruby laser. The data of temperature rise were analyzed by the logarithmic method [24,25]. The thicknesses of the disk samples were corrected for thermal expansion, using the data for unirradiated UO_2 taken from MATPRO-11 [26]. The thermal expansion coefficients of $(U,Gd)O_2$ solid solution with Gd_2O_3 content up to 10 wt% show almost the same as those of UO_2 from room temperature to 2000 K [27], and those of the irradiated samples were assumed to be the same as those of the unirradiated ones. The mass of each sample was measured with an electric balance before and after the thermal diffusivity measurement, which revealed that the mass remained unchanged. For each irradiated sample, three runs of the thermal diffusivity measurement from room temperature to about 1800 K were carried out to study the recovery of the thermal diffusivity.

The thermal conductivity was determined by the equation

$$\lambda_M = \alpha c_p \rho, \tag{1}$$

where λ_M is the thermal conductivity of the sample, α the thermal diffusivity, c_p the specific heat capacity and ρ is the density of the sample. The specific heat capacity of unirradiated UO_2 was taken from MATPRO-11 [26], which was used for both the unirradiated and irradiated UO_2 since the burnup dependence of the specific heat capacity is negligibly small up to 8%FIMA [28]. In the case of UO_2–10 wt%Gd_2O_3, the specific heat capacity was estimated by the Neumann–Kopp rule using the data for UO_2 [26] and those for Gd_2O_3 [29]. The density of each disk sample at the test temperature was corrected for thermal expansion using the data for unirradiated UO_2 [26].

The obtained thermal conductivity was normalized to 96.5% of the theoretical density using the modified Loeb equation [30]

$$\lambda_M = \lambda_{th}(1 - P_\eta), \tag{2}$$

where λ_{th} is the thermal conductivity of the sample with 100% of the theoretical density, P the porosity of the sample and η is the experimental parameter. In the present study, the expression for η reported by Brandt and Neuer [31] was used

$$\eta = 2.6\text{–}5 \times 10^{-4} \quad (T - 273.15), \tag{3}$$

where T is the absolute temperature. The theoretical densities of the irradiated samples were estimated after Ishimoto et al. [11].

3. Results and discussion

3.1. Characteristics of irradiated samples

Fig. 3 shows optical micrographs of polished surfaces of the irradiated samples. In samples D-4_{eq}, E-17_{eq} and F-3_{eq}, bubbles were formed along the grain boundaries, where some of the bubbles were interconnected with each other. Many white spots of the metallic inclusions were seen. These ceramographic features are similar to those observed in the central part of the fuel pellets irradiated in commercial reactors. The temperature escalation during the irradiation test must have caused these features. In sample H-4_{eq}, on the other hand, formations of bubbles and metallic inclusions were not notable compared with those in the other samples. This indicated that sample H-4_{eq} experienced lower temperature than samples D-4_{eq}, E-17_{eq} and F-3_{eq}.

The profiles of fission product distributions were obtained with electron probe microanalysis. Fig. 4 shows relative concentrations of cerium, xenon and cesium along the centerline on the horizontal cross-section of sample D-4_{eq}. The relative concentration was defined as the intensity ratio of characteristic X-rays of a certain element to uranium. The profiles were found to be almost flat. The profiles of the concentrations of the three elements on the vertical cross-section were similar to those on the horizontal cross-section. The profiles obtained for the other samples of H-4_{eq}, E-17_{eq} and F-3_{eq} were almost flat like those of sample D-4_{eq}. The flat profiles of the cerium concentration indicated that the burnup was almost uniform within the sample, since cerium forms chemically stable solid solution with UO_2 which tends to remain unmoving in the fuel even at high temperatures. Furthermore, the flat profiles of the xenon and cesium concentrations indicated that the irradiation temperature was almost uniform within the sample, since xenon and cesium move easily along a temperature gradient.

The lattice parameters of the samples were determined with X-ray diffractometry. Table 1 shows the lattice parameters of samples H-4_{eq}, D-4_{eq}, E-17_{eq} and F-3_{eq}, together with those of unirradiated samples. The lattice parameter increases with an accumulation of irradiation-induced point defects distributed uniformly in the matrix, while it decreases with accumulation of soluble fission products in the matrix when the irradiation-induced point defects are recovered [32]. The lattice parameter increase of sample H-4_{eq} was large compared

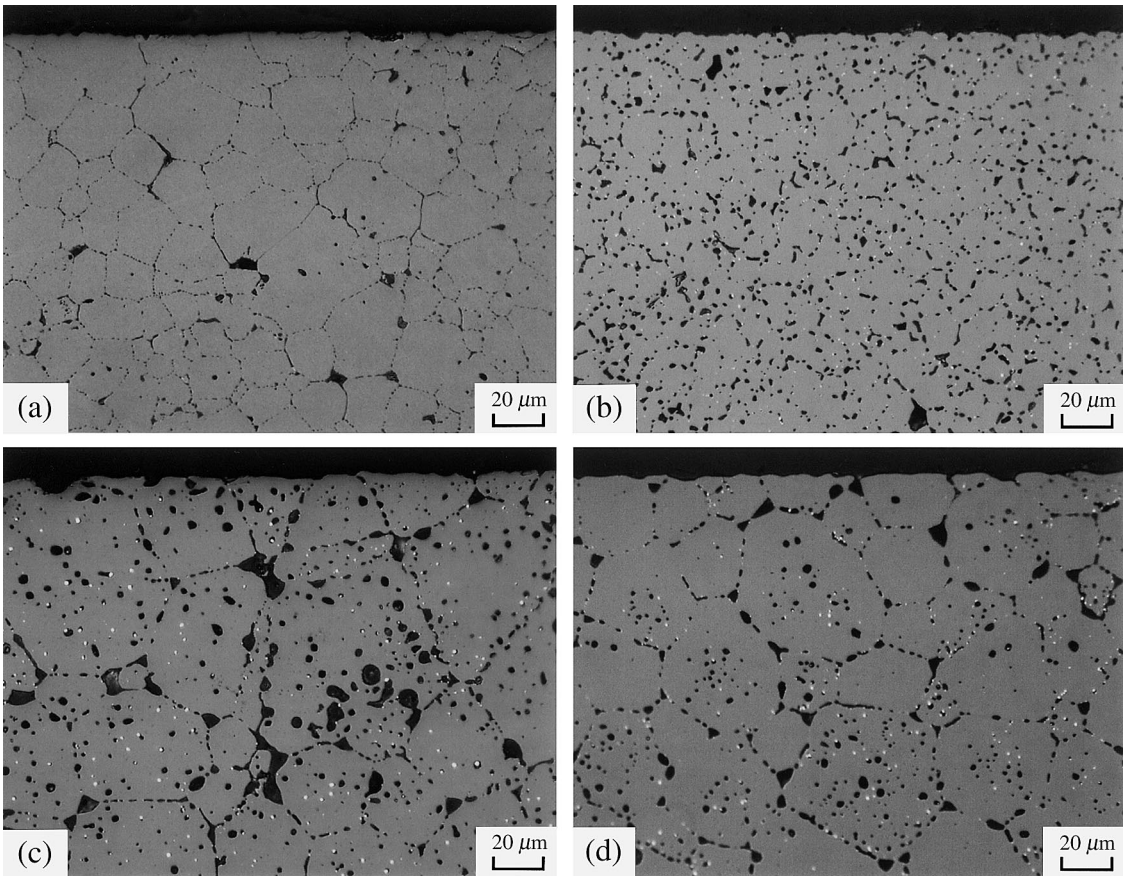

Fig. 3. Optical micrographs of polished surfaces of the irradiated samples: (a) H-4_{eq}, (b) D-4_{eq}, (c) E-17_{eq} and (d) F-3_{eq}.

with those of samples D-4_{eq}, E-17_{eq} and F-3_{eq} though the burnup of sample H-4_{eq} was less than half of those of samples D-4_{eq}, E-17_{eq} and F-3_{eq}. This result indicated that samples D-4_{eq}, E-17_{eq} and F-3_{eq} experienced higher temperatures than sample H-4_{eq} during the temperature escalation, where most of the irradiation-induced point defects in samples D-4_{eq}, E-17_{eq} and F-3_{eq} were recovered. During the low-temperature irradiation after the temperature escalation, the irradiation-induced point defects must have been accumulated in the samples.

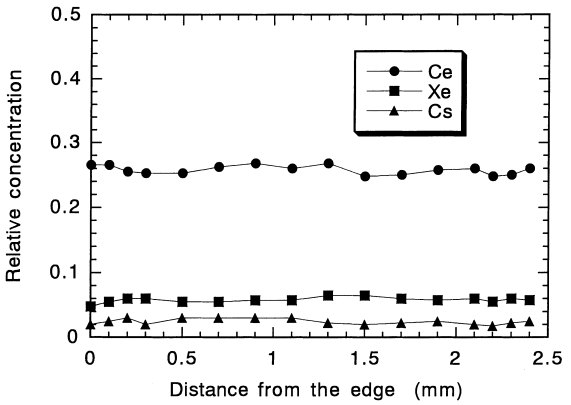

Fig. 4. Relative concentrations of cerium, xenon and cesium along the centerline on the horizontal cross-section of sample D-4_{eq}.

3.2. Thermal conductivities of unirradiated samples

Fig. 5 shows the thermal conductivities of unirradiated UO_2 and UO_2–10 wt%Gd_2O_3 measured on samples H-std and F-std, respectively, as a function of temperature. The figure also shows the reported values for thermal conductivities of UO_2 [4,5,26] and UO_2–10 wt%Gd_2O_3 [5,7] for comparison, where the values were normalized to 96.5% of the theoretical density. The thermal conductivity of unirradiated UO_2 obtained in the present experiment, which was slightly larger than the recommended values by MATPRO-11 [26] and those by Harding and Martin [4], agreed well with the experimental data reported by Hirai and Ishimoto [5]. The

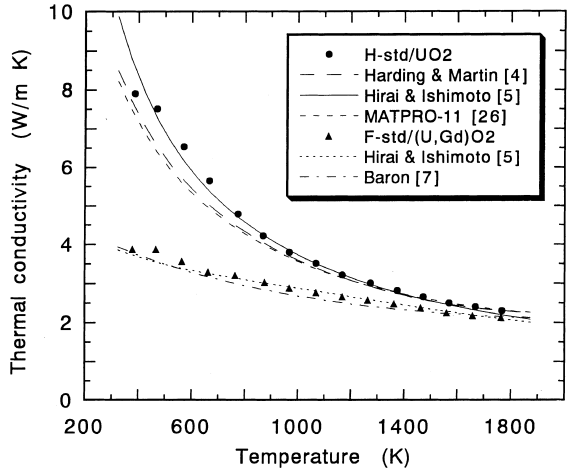

Fig. 5. Thermal conductivities of unirradiated UO_2 and UO_2–10 wt%Gd_2O_3 as a function of temperature, together with the reported values [4,5,7,26]. The values were normalized to 96.5% of the theoretical density.

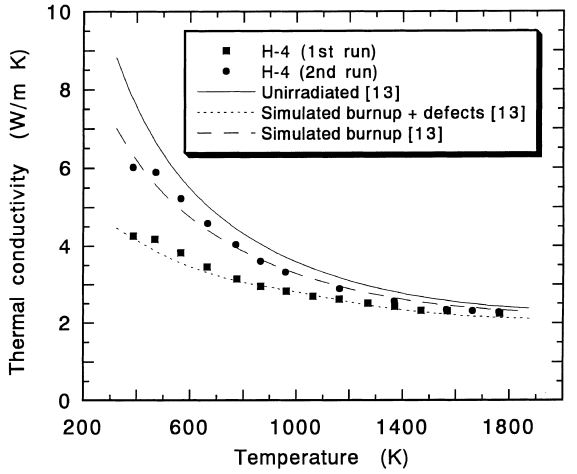

Fig. 6. Thermal conductivities of irradiated UO_2 of sample H-4 as a function of temperature, together with the predicted curves based on the model proposed by Hirai et al. [13]. The values were normalized to 96.5% of the theoretical density.

experimental values obtained by Lucuta et al. [17] were also slightly larger than the recommended values [4,26]. The present experimental values agreed well with those obtained by Lucuta et al. [17]. As for the thermal conductivity of UO_2–10 wt%Gd_2O_3, the present experimental values agreed slightly better with the experimental data reported by Hirai and Ishimoto [5] than with those by Baron and Couty [7] though the difference was small between the data by Hirai and Ishimoto [5] and those by Baron and Couty [7].

3.3. Thermal conductivities of irradiated samples

3.3.1. Irradiated UO_2

Figs. 6–8 show the thermal conductivities of irradiated UO_2 of samples H-4, D-4 and E-17, respectively, as a function of temperature. The results of the first and second runs for each sample are presented in the figures; the result of the third run was almost the same as that of the second run for each sample. In the figures three predicted curves each are also presented, which were drawn based on the model proposed by Hirai et al. [13]; curves for thermal conductivities of unirradiated UO_2, the simulated burnup UO_2 and the simulated burnup UO_2 with irradiation-induced defects, where the values were normalized to 96.5% of the theoretical density. In the model proposed by Hirai et al. [13], the thermal conductivity was assumed to be degraded by (a) fission products dissolved in the UO_2 matrix, (b) irradiation-induced point defects which recover completely above 1100 K and (c) microbubbles which grow above 1400 K. The simulated burnup UO_2 means the UO_2 containing relevant amounts of soluble fission products.

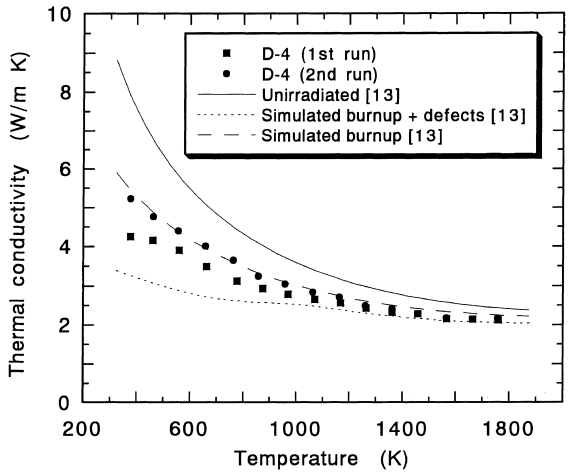

Fig. 7. Thermal conductivities of irradiated UO_2 of sample D-4 as a function of temperature, together with the predicted curves based on the model proposed by Hirai et al. [13]. The values were normalized to 96.5% of the theoretical density.

For sample H-4 shown in Fig. 6, data of the first run were smaller than those of unirradiated UO_2 and were reproduced fairly well by the model [13]. In the second run, the thermal conductivity increased from that in the first run and agreed well with the predicted curve for the simulated burnup UO_2. The increase in the thermal conductivity could be attributed to the recovery of the irradiation-induced point defects during the first run at temperatures up to 1800 K.

In the case of samples D-4 and E-17 shown in Figs. 7 and 8, respectively, the recovery behavior of thermal

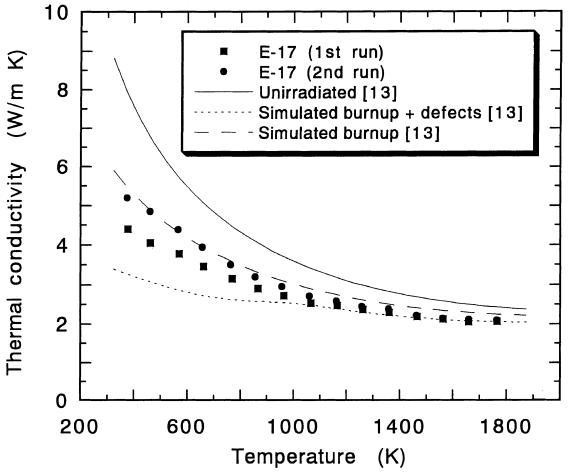

Fig. 8. Thermal conductivities of irradiated UO_2 of sample E-17 as a function of temperature, together with the predicted curves based on the model proposed by Hirai et al. [13]. The values were normalized to 96.5% of the theoretical density.

conductivity was somewhat different from that observed on sample H-4. The thermal conductivities observed in the second runs of samples D-4 and E-17 agreed well with the predicted curve for the simulated burnup UO_2, but those in the first runs were much larger than the predicted curves for the simulated burnup UO_2 with irradiation-induced defects in the temperature range lower than around 1000 K. The lattice parameter increase of samples $D\text{-}4_{eq}$ and $E\text{-}17_{eq}$ measured after the irradiation was small. Since these samples experienced higher temperature than 1273 K during the temperature escalation, most of the irradiation-induced point defects accumulated before the escalation may have been recovered. This assumption was supported by the fact that the irradiated UO_2 pellet, which experienced a power-ramp in a material testing reactor after base irradiation in a commercial reactor, showed no clear recovery of the thermal conductivity in the second run of the measurement by the laser flash method and that the thermal conductivity agreed well with the predicted curve for the simulated burnup UO_2 [16]. The temperature at the power-lamp was estimated to be 1300 K [16]. The irradiation-induced point defects presented in samples D-4 and E-17 at the first runs were, therefore, accumulated mainly after the temperature escalation, so the reduction of the thermal conductivities attributable to the irradiation-induced point defects was smaller than that predicted by the model.

As the irradiation conditions for samples D-4 and E-17 were almost the same, it was considered to be possible to check the effect of grain size on the thermal conductivity of UO_2. The recovery behaviors and the values themselves of the thermal conductivity for samples D-4 and E-17 were almost the same, as shown in Figs. 7 and 8. No effect of the grain size was explicitly observed as expected.

Besides the model proposed by Hirai et al. [13], two models are available which take account of the irradiation-induced defects and their recovery in the calculation of the thermal conductivity; the model proposed by Lucuta et al. [17] and the Baron-Hervé-97 model [19]. Figs. 9 and 10 compare those models with the present experimental values of samples H-4 and D-4, respectively, where the values were normalized to 96.5% of the theoretical density. In the Baron-Hervé-97 model [19], the lattice parameter is used as a marker of the damage state of the material. In the present study, lattice parameters used for the thermal conductivity calculation were measured or estimated values. As the lattice parameters of the samples were measured only before the thermal diffusivity measurement, as shown in Table 1, the lattice parameters after the recovery of the irradiation-induced point defects were estimated by the equation proposed by Une et al. [32].

By using the model proposed by Lucuta et al. [17], the present experimental data on the thermal conductivities of samples H-4 and D-4 after the recovery of the irradiation-induced point defects could be reproduced fairly well. As for the thermal conductivity before the recovery, the model prediction agreed considerably well with the data of sample H-4 in a relatively low-temperature range, while the predicted curve distinctively disagreed with the data of sample D-4 in a relatively low-temperature region. This disagreement could be explained by the assumption that the irradiation-induced point defects accumulated in sample D-4 before the temperature escalation were recovered during the temperature esca-

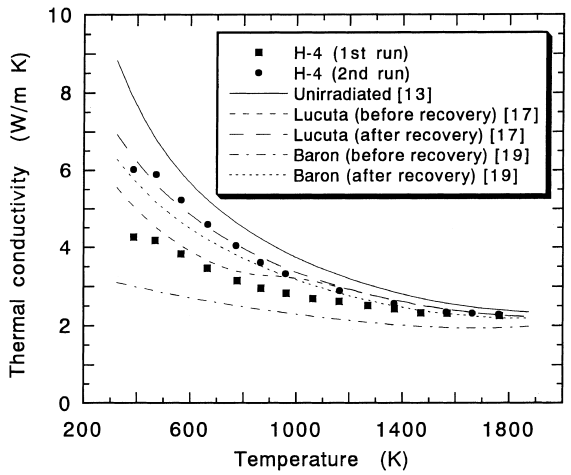

Fig. 9. Comparison of the predicted curves based on the model proposed by Lucuta et al. [17] and the Baron-Hervé-97 model [19] with the thermal conductivities of irradiated UO_2 of sample H-4 as a function of temperature. The values were normalized to 96.5% of the theoretical density.

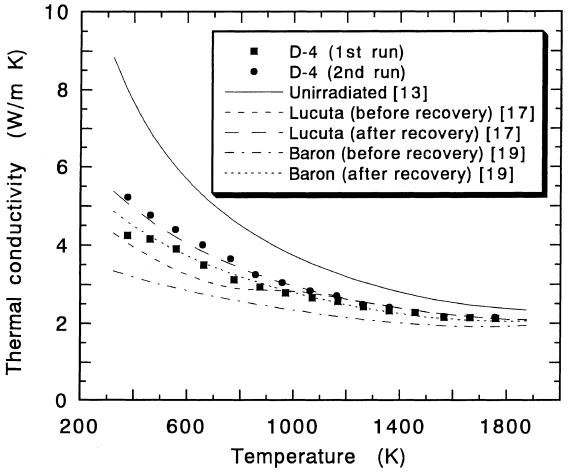

Fig. 10. Comparison of the predicted curves based on the model proposed by Lucuta et al. [17] and the Baron-Hervé-97 model [19] with the thermal conductivities of irradiated UO_2 of sample D-4 as a function of temperature. The values were normalized to 96.5% of the theoretical density.

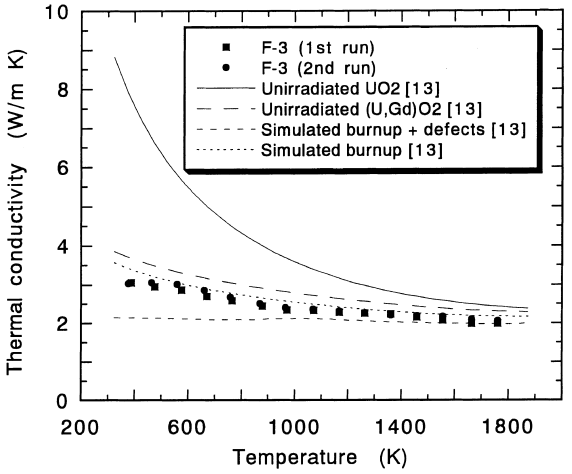

Fig. 11. Thermal conductivities of irradiated UO_2–10 wt%Gd_2O_3 of sample F-3 as a function of temperature, together with the predicted curves based on the model proposed by Hirai et al. [13]. The values were normalized to 96.5% of the theoretical density.

lation. It was shown that the Baron-Hervé-97 model [19] underestimates the thermal conductivities for both the samples. Especially, the degree of underestimation was large in the thermal conductivity before the recovery of the irradiation-induced point defects.

3.3.2. Irradiated UO_2–10 wt%Gd_2O_3

Fig. 11 shows thermal conductivities of irradiated UO_2–10 wt%Gd_2O_3 of sample F-3 as a function of temperature. The results of the first and second runs are presented in the figure; the result of the third run was almost the same as that of the second run. In the figure, four predicted curves are also presented, which were drawn based on the model proposed by Hirai et al. [13]; curves for thermal conductivities of unirradiated UO_2, unirradiated UO_2–10 wt%Gd_2O_3, the simulated burnup UO_2–10 wt%Gd_2O_3 and the simulated burnup UO_2–10 wt%Gd_2O_3 with irradiation-induced defects, where the values were normalized to 96.5% of the theoretical density. The model proposed by Hirai et al. [13] used for the thermal conductivity calculation of UO_2–10 wt%Gd_2O_3 was basically the same as that used for UO_2 in Section 3.3.1. In the present case, Gd was an additional factor that degrades the thermal conductivity of UO_2.

The thermal conductivity obtained in the first run was slightly smaller than that in the second run and could not be reproduced by the model calculation. The thermal conductivity obtained in the second run as well as that in the first run nearly agreed with the predicted curve for the simulated burnup UO_2–10 wt%Gd_2O_3. The disagreement between the thermal conductivity obtained in the first run and the predicted curve for the simulated burnup with irradiation-induced defects was observed in sample F-3, which was also observed in samples D-4 and E-17. The lattice parameter increase of sample F-3_{eq} measured after the irradiation was also small. It is estimated that, like samples D-4 and E-17, the irradiation-induced point defects in sample F-3 were recovered during the temperature escalation, and that the irradiation-induced point defects responsible for the reduction of thermal conductivity in the first run were accumulated mainly after the temperature escalation.

4. Conclusions

The disk-shaped UO_2 and UO_2–10 wt%Gd_2O_3 samples were prepared and irradiated to about 4%FIMA in the research reactor to measure the thermal diffusivities by the laser flash method from room temperature to about 1800 K. The burnup was almost uniform within each sample. The irradiation temperature was almost constant and uniform within each sample except the temperature escalation that occurred during the irradiation. The thermal conductivities were determined from the measured thermal diffusivities and densities and the specific heat capacities in the literature. The following was concluded:

1. The thermal conductivity decreased by irradiation, while it partly recovered after the thermal diffusivity measurement at temperatures up to about 1800 K. The recovery of the thermal conductivity was explained by the recovery of the irradiation-induced point defects during the measurement.

2. The thermal conductivity reduction attributable to the irradiation-induced point defects was small in the samples which experienced higher temperature than 1273 K during the temperature escalation, whose lattice parameter increase was small measured after the irradiation.
3. The present results of the thermal conductivity measurements were reproduced considerably well by using the model proposed by Hirai et al., which takes account of the effects of soluble fission products, irradiation-induced defects and gadolinium content.

Acknowledgements

The authors wish to express their thanks to Messrs I. Owada, S. Miyata, H. Sekino, A. Ishikawa and T. Tomita, Department of Hot Laboratories, JAERI, for their cooperation in the post-irradiation examinations. The authors are indebted to Mr T. Kikuchi, Department of Engineering Services, JAERI, for the irradiation capsule fabrication, and to Mr M. Aizawa, Department of Research Reactor, JAERI, for the irradiation test. Thanks are also given to Dr K. Fukuda, former Head of Fuel Irradiation and Analysis Laboratory, JAERI, for his interest and encouragement.

References

[1] A.B.G. Washington, Preferred values for the thermal conductivity of sintered ceramic fuel for fast reactor use, UK Atomic Energy Authority, TRG Report 2236(D), 1973.
[2] D.G. Martin, J. Nucl. Mater. 110 (1982) 73.
[3] G.J. Hyland, J. Nucl. Mater. 113 (1983) 125.
[4] J.H. Harding, D.G. Martin, J. Nucl. Mater. 166 (1989) 223.
[5] M. Hirai, S. Ishimoto, J. Nucl. Sci. Technol. 28 (1991) 995.
[6] M. Amaya, M. Hirai, T. Kubo, Y. Korei, J. Nucl. Mater. 231 (1996) 29.
[7] D. Baron, J.C. Couty, in: Proceedings of the IAEA Technical Committee Meeting, Windermere, United Kingdom, 19–23 September 1994, IAEA-TECDOC-957, International Atomic Energy Agency, 1995, p. 229.
[8] P.G. Lucuta, Hj. Matzke, R.A. Verrall, H.A. Tasman, J. Nucl. Mater. 188 (1992) 198.
[9] P.G. Lucuta, Hj. Matzke, R.A. Verrall, J. Nucl. Mater. 217 (1994) 279.
[10] P.G. Lucuta, Hj. Matzke, R.A. Verrall, J. Nucl. Mater. 223 (1995) 51.
[11] S. Ishimoto, M. Hirai, K. Ito, Y. Korei, J. Nucl. Sci. Technol. 31 (1994) 796.
[12] M. Amaya, M. Hirai, J. Nucl. Mater. 246 (1996) 158.
[13] M. Hirai, M. Amaya, T. Matsuura, M. Nomata, H. Hayashi, M. Kitamura, in: Proceedings of the IAEA Technical Committee Meeting, Tokyo, Japan, October 28–November 1, 1996, IAEA-TECDOC-1036, International Atomic Energy Agency, 1998, p. 139.
[14] J. Nakamura, M. Uchida, H. Uetsuka, T. Furuta, in: Proceedings of the IAEA Technical Committee Meeting, Tokyo, Japan, October 28–November 1, 1996, IAEA-TECDOC-1036, International Atomic Energy Agency, 1998, p. 127.
[15] T.L. Shaw, J.C. Carrol, R.A. Gomme, in: Proceedings of the IAEA Technical Committee Meeting, Tokyo, Japan, October 28–November 1, 1996, IAEA-TECDOC-1036, International Atomic Energy Agency, 1998, p. 115.
[16] M. Amaya, M. Hirai, Y. Wakashima, T. Kubo, T. Kogai, H. Hayashi, M. Kitamura, in: Proceedings of the TopFuel '97, Manchester, United Kingdom, 9–11 June 1997, British Nuclear Energy Society, 1997, p. 236.
[17] P.G. Lucuta, Hj. Matzke, I.J. Hastings, J. Nucl. Mater. 232 (1996) 166.
[18] M. Amaya, M. Hirai, J. Nucl. Mater. 247 (1997) 76.
[19] D. Baron, in: Proceedings of the Seminar on Thermal Performance of High Burn-up LWR Fuel, Cadarache, France, 3–6 March 1998, Nuclear Energy Agency, 1998, p. 129.
[20] R.C. Daniel, I. Cohen, In-pile effective thermal conductivity of oxide fuel elements to high fission depletions, Bettis Atomic Power, Report WAPD-246, 1964.
[21] J.A.L. Robertson, A.M. Ross, M.J.F. Notley, J.R. MacEwan, J. Nucl. Mater. 7 (1962) 223.
[22] W. Wiesenack, in: Proceedings of the 1997 International Topical Meeting on LWR Fuel Performance, Portland, USA, 2–6 March 1997, American Nuclear Society, 1997, p. 507.
[23] I. Owada, Y. Nishino, T. Kushida, J. Nakamura, T. Matsuda, Characterization test of the pellet thermal conductivity measurement apparatus using unirradiated samples, Japan Atomic Energy Research Institute, Report JAERI-Tech 94-028, 1994.
[24] H.M. James, J. Appl. Phys. 51 (1980) 4666.
[25] Y. Takahashi, K. Yamamoto, T. Ohsato, Netsu Sokutei 15 (1988) 103.
[26] D.L. Hagrman, G.A. Reymann, MATPRO Version-11: A handbook of materials properties for use in the analysis of light water reactor rod behavior, EG & G Idaho, Inc., Report NUREG/CR-0497, TREE-1280, 1979.
[27] K. Une, J. Nucl. Sci. Technol. 23 (1986) 1020.
[28] R.A. Verrall, P.G. Lucuta, J. Nucl. Mater. 228 (1996) 251.
[29] L.B. Pankratz, E.G. King, K.K. Kelley, High-temperature heat contents and entropies of sesquioxides of europium, gadolinium, neodymium, samarium, and yttrium, US Department of the Interior, Report of Investigations 6033, 1961.
[30] A.L. Loeb, J. Am. Ceram. Soc. 37 (1954) 96.
[31] R. Brandt, G. Neuer, J. Non-Equilib. Thermodyn. 1 (1976) 3.
[32] K. Une, Y. Tominaga, S. Kashibe, J. Nucl. Sci. Technol. 28 (1991) 409.